S31A-1688

Kinematic Source Inversion using Strong Motion Data Considering Three-Dimensional Fault Geometry

Kimiyuki ASANO and Tomotaka IWATA
(Disaster Prevention Research Institute, Kyoto University, JAPAN)
E-mail: k-asano@egmdpri01.dpri.kyoto-u.ac.jp

Motivation

Near-source strong ground motions during large earthquakes are governed by spatiotemporal slip progression on the fault plane. Many previous studies succeeded to obtain precise slip distributions of large earthquakes from strong motion and other seismic and geodetic data set.

The geometry of source fault is also known to be important to quantitatively explain near-source strong ground motions (e.g., Iwata et al., 2000; Gallovič et al., 2009). However, most of source inversion studies except special cases assumed one or plural planar fault planes in their kinematic inversion analyses. In recent studies on the detailed aftershock relocations for large earthquakes, it is known that the geometry of the source fault is complex rather than simple planar shape (e.g., Kato et al., 2005).

In order to include effects of fault geometry on near-source ground motions, we are trying to develop a method to invert slip distribution with its fault geometry. The proposed method is applied to the 2008 Iwate-Miyagi Nairiku earthquake, which is a M_W 6.9 inland crustal earthquake occurring in northeast Japan.

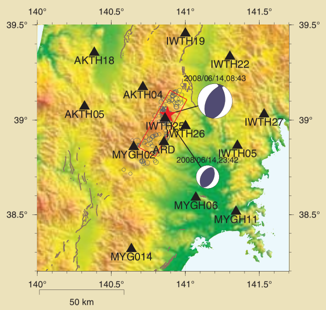

Fig.1 Map showing the strong motion stations used in this study. Open circles indicate epicenters of aftershocks within 1 hour after the mainshock.

Method

1st step

Conventional Linear Waveform Inversion
(e.g., Hartzell and Heaton, 1983)

Spatiotemporal slip history on a single planar fault model is solved using the multiple window linear waveform inversion method.

2nd step

Nonlinear Waveform Inversion

Strike and dip angles at control points are simultaneously solved with the slip amounts at each time-window at each subfault by the iterative inversion using the Lavenberg-Marquardt method.

The initial model of the 2nd step is the solution of the 1st step.

The geometry of the source fault is represented by strike and dip angles at some control points. Then, strike and dip angles for individual subfault are set by bilinear interpolation.

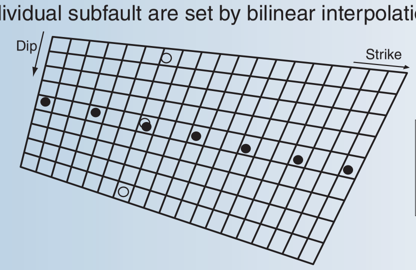

Fig.2 Schematic illustration of the three-dimensional source fault model. Solid and open circles indicate the location of the control point for the strike and dip angles, respectively.

Velocity Structure Model

It is quite important for obtaining a reliable source model from observed data to use appropriate Green's functions. So we use a set of station-dependent velocity structure models to calculate Green's functions for each station. The one-dimensional layered velocity structure is modeled for each strong motion station by waveform modeling of aftershock records following the procedure by Asano and Iwata (2009).

Firstly, the reference velocity structure model, which is used for all stations, is assumed. Then, thicknesses of sedimentary layers are estimated for each station by simulating waveforms for a moderate aftershock event using GA. For deeper part (crust and mantle), horizontal layered structure is assumed based on the refraction survey by Iwasaki et al. (2001).

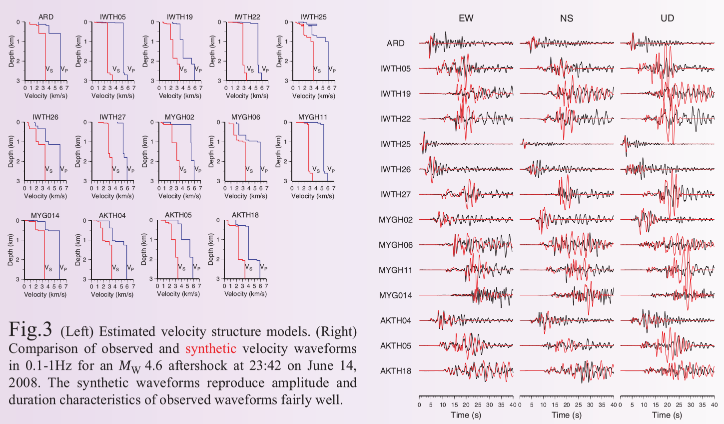

Fig.3 (Left) Estimated velocity structure models. (Right) Comparison of observed and synthetic velocity waveforms in 0.1-1Hz for an M_W 4.6 aftershock at 23:42 on June 14, 2008. The synthetic waveforms reproduce amplitude and duration characteristics of observed waveforms fairly well.

Inversion Results

Single planar fault model

The strike and dip angles of the fault plane are fixed at 209° and 51°, respectively (from F-net moment tensor solution by NIED).

Seismic Moment: 2.89×10^{19} Nm (M_W 6.9)
Maximum Slip: 6.4 m (in shallower asperity)
Average Slip: 1.3 m
The rupture propagation velocity of the first time window: 2.4 km/s (~ 0.7β)

Final slip distribution

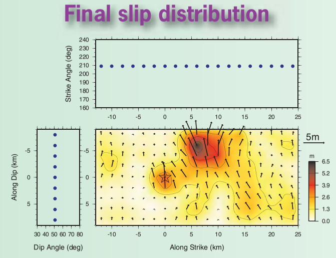

Fig.4 Final slip distribution on the fault for the planar fault model. The arrows show the slip vectors of the hanging wall relative to the foot wall. The open star indicates the hypocenter or rupture starting point.

Waveform fitting

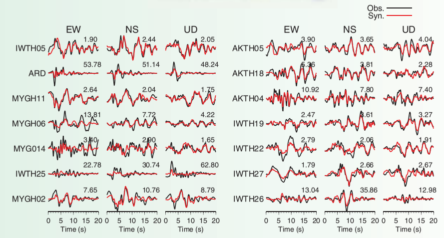

Fig.5 Comparison between the observed and synthetic velocity waveforms in 0.1-1Hz for the planar fault model. The number is maximum amplitude of observation in cm/s.

Variable strike and dip model

Here, we are showing the source model obtained after 20 iterations.

Seismic Moment: 3.29×10^{19} Nm (M_W 6.9)
Maximum Slip: 5.3 m (in shallower asperity)
Average Slip: 1.4 m
The rupture propagation velocity of the first time window: 2.4 km/s (~ 0.7β)

cf. Seismic Moment by the Global CMT: 2.58×10^{19} Nm (M_W 6.9)

The asperity or large slip area is found in the south shallow portion of the fault plane (4 ~ 10 km southeast of the epicenter).

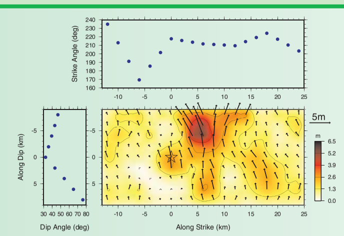

Fig.6 Final slip distribution on the fault for the variable strike and dip model.

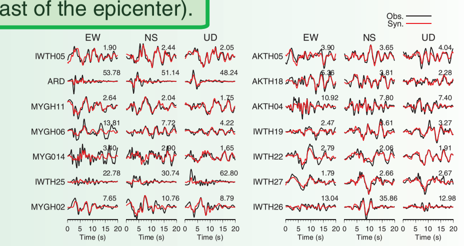

Fig.7 Comparison between the observed and synthetic velocity waveforms in 0.1-1Hz for the variable strike and dip moel. Waveform fit for ARD and IWTH22 are improved in this model.

<< Assumption for the Source Inversion >>
- The S-wave portion of the velocity waveforms in 0.1-1Hz observed at 14 strong motion stations.
- Rupture starting point is fixed at the hypocenter (39.0298°N, 140.8807°E, 7.77km), which was determined by JMA.
- The temporal history of the moment release at each subfault is expressed by a series of eight smoothed ramp functions with the rise time of 1.0 s, each separated by 0.5 s.
- Green's function is calculated by the discrete wavenumber method (Bouchon, 1981) with the reflection/transmission matrix (Kennett and Kerry, 1979).
- Relative strength of spatiotemporal smoothing constraint is determined by the ABIC minimization criterion (Sekiguchi et al., 2000)

Surface Rupture and Aftershocks

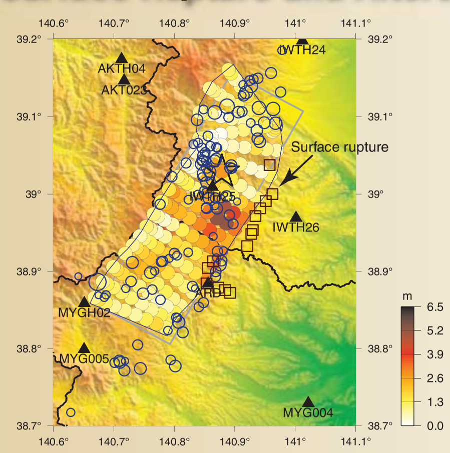

Fig.8 Comparison among slip distribution, aftershocks and surface ruptures. The open star indicates the epicenter of the mainshock. The open circles are the epicenter of aftershocks within 1 hour after the mainshock by JMA. The open squares indicate the locations of surface rupture associated with this event reported by AFRC/GSJ (2008). A part of surface rupture seems to correspond the shallower asperity obtained by the waveform inversion. Most of aftershocks occurred outside the asperities.

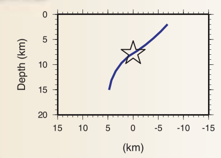

Fig.9 Geometry of the source model derived by out study in the dip direction.

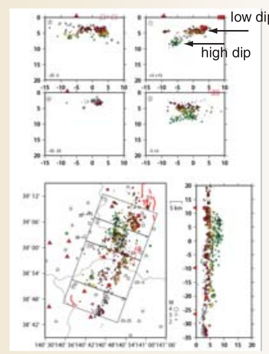

Fig.10 Relocated Aftershock distribution by Tohoku Univ. (2008).

Conclusions

We proposed a method to estimate the spatiotemporal slip history with unknown fault geometry from strong motion data, and applied to the data set of the 2008 Iwate-Miyagi Nairiku earthquake.

The obtained fault geometry appears to be consistent with the detailed aftershock distribution and the surface rupture observations.

We may improve the constraint for the fault geometry by including geodeic data (e.g. static GPS data).

Acknowledgments

We are deeply indebted to K-NET and KiK-net operated by the National Research Institute for Earth Science and Disaster Prevention (NIED) for the strong motion data, and the Kurihara Dam Management Office, Miyagi prefecture for the strong motion data at the Aratozawa Dam. We also used the hypocenter catalog of JMA, and the moment tensor solution catalog of F-net by NIED.

References

Asano and Iwata (2009), *Bull. Seism. Soc. Am.*, **99**, 123-140.
Bouchon (1981), *Bull. Seism. Soc. Am.*, **71**, 959-971.
Gallovič *et al.* (2009), *J. Geophys. Res.*, **114**, doi:10.1029/2008JB006171.
Hartzell and Heaton (1983), *Bull. Seism. Soc. Am.*, **73**, 1553-1583.
Iwasaki *et al.* (2001), *Geophys. Res. Lett.*, **28**, 3239-2332.
Iwata *et al.* (2000), *Eos Trans. AGU*, **81**(48), Fall Meet. Suppl., Abstract S72B-07.
Kato et al. (2005), Geophys. Res. Lett., 32, L07307, doi:10.1029/2005GL022366.
Kennett and Kerry (1979), *Geophys. J. Roy Astr. Soc.*, **57**, 557-583.
Ripperger and Mai (2004), *Geophys. Res. Lett*, **31**(18), L18610.
Sekiguchi *et al.* (2000), *Bull. Seism. Soc. Am.*, **90**, 117-133.
AFRC, GSJ, AIST (2008), *http://unit.aist.go.jp/actfault/katsudo/jishin/iwate_miyagi/index.html*